Thymoquinone Oxime Synthesis and Its Effects on Melanoma Cells: Cytotoxic, Genotoxic, and Apoptotic Evaluation

Abstract

Strong evidence supports the anticancer properties of natural plant product isolates. The cytotoxic, genotoxic, and apoptotic properties of an oxime derivative of thymoquinone (TQ) in melanoma cancer cells were investigated.

The structure of TQ-Oxime was elucidated through nuclear magnetic resonance, and its effect on B16F10 and L929 cell lines was assessed using a luminometric adenosine triphosphate assay. Intracellular reactive oxygen species (iROS) were quantified via fluorometry, mitochondrial membrane potential (MMP) was assessed using flow cytometry, glutathione (GSH) levels were measured using a luminometric GSH/oxidized glutathione assay, DNA damage via comet assay, and apoptosis was detected using acridine orange/ethidium bromide staining.

Concentrations (0.5-20 μM) of TQ-Oxime significantly increased cytotoxicity, DNA damage, apoptosis, and iROS, in a concentration-dependent manner compared (p<0.001). In addition, MMP and GSH levels decreased significantly with increasing concentrations compared with the control (p<0.001).

Overall, these findings contribute to our understanding of the therapeutic potential of TQ and its derivatives in cancer treatment.

Keywords*: apoptosis, genotoxicity, melanoma cancer, thymoquinone-oxime*

3. Experimental

3.1. Materials and equipment

Thymol (Cas number 89-83-8, ≥98% purity) was provided by Merck KGaA. Most other chemicals were supplied by Sigma-Aldrich (St. Louis, MO, USA). ^{1}H-NMR and ^{13}C-NMR spectra were recorded on a Bruker Avance III 500 MHz Three-channel NMR spectrometer. C, H and N microanalyses were performed on the LECO, CHNS-932 elemental analyzer. Mass spectra were recorded on Bruker Microflex LT MALDI-TOF MS spectrometer using α-cyano-4-hydroxycinnamic acid (CHCA) as the MALDI matrix.

3.2. Synthesis of TQ-Ox

Commercial thymol was purchased from Sigma-Aldrich, and thymoquinone-oxime (TQ-Ox) was synthesized by the method mentioned in the article by (Kale et al., 2022).

The ^{1}H-NMR analysis for Thymol: ^{1}H-NMR (DMSO-d_6, 600 MHz) δ 8.91 (s, 1H), 6.83 (dd, *J* = 7.8, 2.6 Hz, 1H), 6.51 (dd, *J* = 5.7, 1.9 Hz, 1H), 6.41 (dd, *J* = 7.6, 2.3 Hz, 1H), 3.07 (dt, *J* = 13.5, 6.6 Hz, 1H), 2.05 (d, *J* = 3.7 Hz, 3H), 1.03 (dq, *J* = 7.1, 2.3 Hz, 6H). The NMR data of the thymol is consistent with the NMR data in the study by Tang et al. (Tang & Hou, 2011).

The ^{1}H-NMR analysis for Thymoquinone: ^{1}H-NMR (DMSO-d_6, 600 MHz) δ 6.73-6.70 (m, 1H), 6.58 – 6.55 (m, 1H), 2.89 (ttd, *J* = 9.6, 4.7, 2.6 Hz, 1H), 1.95 (dt, *J* = 3.2, 1.8 Hz, 3H), 1.06 (ddd, *J* = 5.2, 2.8, 1.4 Hz, 6H). The NMR data of the thymoquinone is consistent with the NMR data in the study by Gour et al. (Gour et al., 2023).

For TQ-Ox synthesis, 3.00 g (19.97 mmol) of thymol was dissolved in a mixture of 30 mL HCl and 30 mL ethanol. 1.40 g of $NaNO_2$ was slowly added to the reaction medium at 0°C and stirred for 1 hour at the same temperature. 5 mL of ethanol was then added, and the reaction was stirred for another hour at room temperature. The reaction mixture was diluted with water and extracted with diethyl ether. The organic phase was extracted with a 10% aqueous Na_2CO_3 solution. Acidification of the carbonate solution with HCl resulted in the formation of a yellow precipitate. This yellow precipitate was filtered and washed extensively with hexane to purify. Yield: 2.64 g (67%), m.p.: 155 °C. Anal. Calc. for $C_{10}H_{13}NO_2$: C, 67.02; H, 7.31; N, 7.82%, found: C, 67.01; H, 7.29; N, 7.79%. ^{1}H-NMR (d-DMSO, δ, ppm) 13.39 (s, 1H), 7.44 (s, 1H), 6.26 (s, 1H), 2.91 (m, 1H), 2.15 (s, 3H), 1.04 (d, *J* = 6.8 Hz, 6H). ^{13}C-NMR (d-DMSO) δ 186.38, 149.91, 147.93, 146.65, 128.61, 118.32, 26.70, 21.92, and 17.18. MALDI-TOF (*m/z*):

Calc. 179.22, found as 368.01 $[M + CHCA]^+$, 352.378 $[M - OH + CHCA]^+$ and 391.02 $[M + CHCA + Na]^+$.

3.3. Characterization of TQ-Ox

The characterization of TQ-Ox was performed using a Bruker Avance III 500 MHz Three channel NMR spectrometer and is detailed in the experimental section of the Supplementary file. Proton and carbon NMR spectra were recorded in deuterated DMSO (DMSO-d6). The aromatic and aliphatic peaks are well-defined and confirm the structure of TQ-Ox.

3.4. Cytotoxicity, intracellular ROS, MMP, and intracellular GSH levels

3.4.1. Cell maintenance

Dulbecco's Modified Eagle's Medium, Minimum Essential Medium Eagle's medium, 10% fetal bovine serum (FBS), and 1% Penicillin-Streptomycin (P/S) were used to grow malignant melanoma (B16F10, CRL-6475™) cells to demonstrate the efficacy of the elucidated candidate anti-cancer agent and healthy fibroblast (NCTC clone 929 [L cell, L-929, derivative of Strain L], CCL-1) cells to determine whether it has selectivity against cancer. The cell lines were purchased from the American Type Culture Collection.

3.4.2. Cytotoxicity

The cytotoxicity of TQ-Ox on B16F10 and L929 cell lines was evaluated using the ATP assay (CellTiter-Glo®; cat #G7570, Promega, Madison, WI). Cell lines were seeded 6 $x10^3$ cells per well in 96- opaque white well plates. The seeded cell lines were treated with TQ-Ox concentrations of 0.5-20 μM and incubated at 37°C in 5% CO_2. After 24 hours of incubation, 100 uL ATP solution was added to each well and incubated for 10 minutes. Cytotoxicity was then measured with a Flash Multimode Reader (BioTek, Synergy™, HTX, USA), and the results were expressed in luminescence units (RLU).

3.4.3. Intracellular ROS

Intracellular ROS production was assessed using the fluorescent signal indicator 2,7-dichlorodihydrofluoresceindiacetate (H_2DCF-DA; Sigma Aldrich, Germany). TQ-Ox (0.5-20 μM) was added to 6$x10^3$ cells per well seeded on 96 black opaque well plates and incubated for 24 hours. After incubation, the media were aspirated, and the wells were washed three times with 1x Dulbecco's Phosphate Buffered Saline (dPBS). 100 μL of 10 μM H_2DCF-DA was

added and incubated for 30 minutes at 37℃ in an incubator. The fluorescence intensity of DCF formed after incubation was measured using an Ex:488nm/Em:525nm fluorescence plate reader (BioTek, Synergy™, HTX, USA). The results were calculated as iROS/ATP and expressed as relative fluorescence units (RFU).

3.4.4. Mitochondrial Membrane Potential

Decreased MMP indicates loss of mitochondrial membrane integrity, reflecting the initiation of proapoptotic signaling. After TQ-Ox was removed and washed after 24 hours of incubation, cells were incubated with 40 nM $DiOC_6(3)$ (Sigma Aldrich, Germany) at 37℃ for 15 minutes and washed with 1x PBS. After washing, the cells were analyzed by flow cytometry (Becton Dickinson, FACS Canto II) (λexc\λem:484/501 nm). MMP was expressed as Δψm.

3.4.5. Intracellular Glutathione Level

GSH-GloTM Glutathione Assay (cat #V6611; Promega, Madison, WI), a luminescent glutathione kit, reduces glutathione with the enzyme glutathione s transferase and converts the substrate luciferin-NT to luciferin. The 6 $x10^3$ cells per well were seeded onto 96 opaque-white well plates. The wells were treated with 0.5 - 4 μM concentrations of TQ-Ox for 24 hours. 50 μL of glutathione reagent was added and incubated at 24℃ for 5 minutes. Subsequently, 100 μL of Luciferin Reagent was added to each well, and the levels of GSH were measured in a Multimode Flash Reader (Thermo, Waltham, USA). The results were expressed as % relative luminescence (RLU).

3.5. Apoptosis and DNA damage Analysis

3.5.1 Apoptosis

As mentioned before, apoptosis was detected by acridine orange/ethidium bromide (AO/EB) stain by McGahon et al. (McGahon et al., 1995). Using a fluorescence microscope (Nikon Eclipse Ts2, Japan), a minimum of 100 cells were counted, and nuclear morphology changes on B16F10 and L929 cells were conducted to assess alterations in the structure and appearance of the cell nucleus.

3.5.2 DNA Damage

DNA damage was performed by the Comet assay method (Singh et al., 1990). In brief, the experimental procedure was involved seeding the cells in tissue culture flasks followed by an

incubation period. Subsequently, the cells were suspended in 0.65% low melting point agarose, and the resulting cellular suspension was evenly spread onto microscope slides pre-coated with 1% normal-melting point agarose. Following cell lysis, electrophoresis was performed to induce DNA migration. The samples were then neutralized, fixed, and subjected to staining with Ethidium Bromide solution (Sigma Aldrich, Germany). Fluorescence microscopy was employed to capture images of the DNA tails, and the Comet Assay IV analysis program (Leica DM 1000, Solms, Germany) was utilized to quantify the percentage of DNA tails observed in the images. By analyzing these percentages, the extent of DNA damage was determined, providing insights into the genotoxic effects of the experimental conditions.

3.6. *In silico* molecular docking

Autodock Vina (Trott & Olson 2009) was used to estimate how strongly thymoquinone-oxime (TQ-Ox) binds to tyrosinase in a molecular docking study. The 3D structure of TQ-Ox was optimized using Avogadro software. The X-ray crystal structure of tyrosinase (PDB: 2Y9W) was downloaded from the RCSB Protein Data Bank. Water molecules were removed from the protein structure, and polar hydrogens and Kollman charges were added (Trott & Olson, 2009). The amino acids in the active site of tyrosinase was identified using Discovery Studio Visualizer 2021. The Lamarckian Genetic Algorithm was chosen as the docking engine, with all parameters set to default (Morris et al. 1998). The inhibitors with the lowest energy docking score were selected from 10 conformations generated by Autodock Vina. Discovery Studio Visualizer 2021 and UCSF Chimera 1.13.1 were used to visualize the 2D and 3D figures.

3.7. Statistical Analysis

The SPSS version 25.0 program (IBM, Armonk, NY, USA) was used for all statistical calculations. Nonparametric data were expressed as interquartile ranges, and parametric data as mean standard deviation (SD) (IQR). A Mann-Whitney *U* test was used to determine differences between two parameters within groups. The Kruskal-Wallis test was used to compare two or more independent parameters. Categorical data were evaluated using the chi-square test. The $p<0.05$ was considered statistically significant. The IC_{50} values of each cell line were calculated with the GraphPad Prism Version 9.5.1 program.

Figure S1

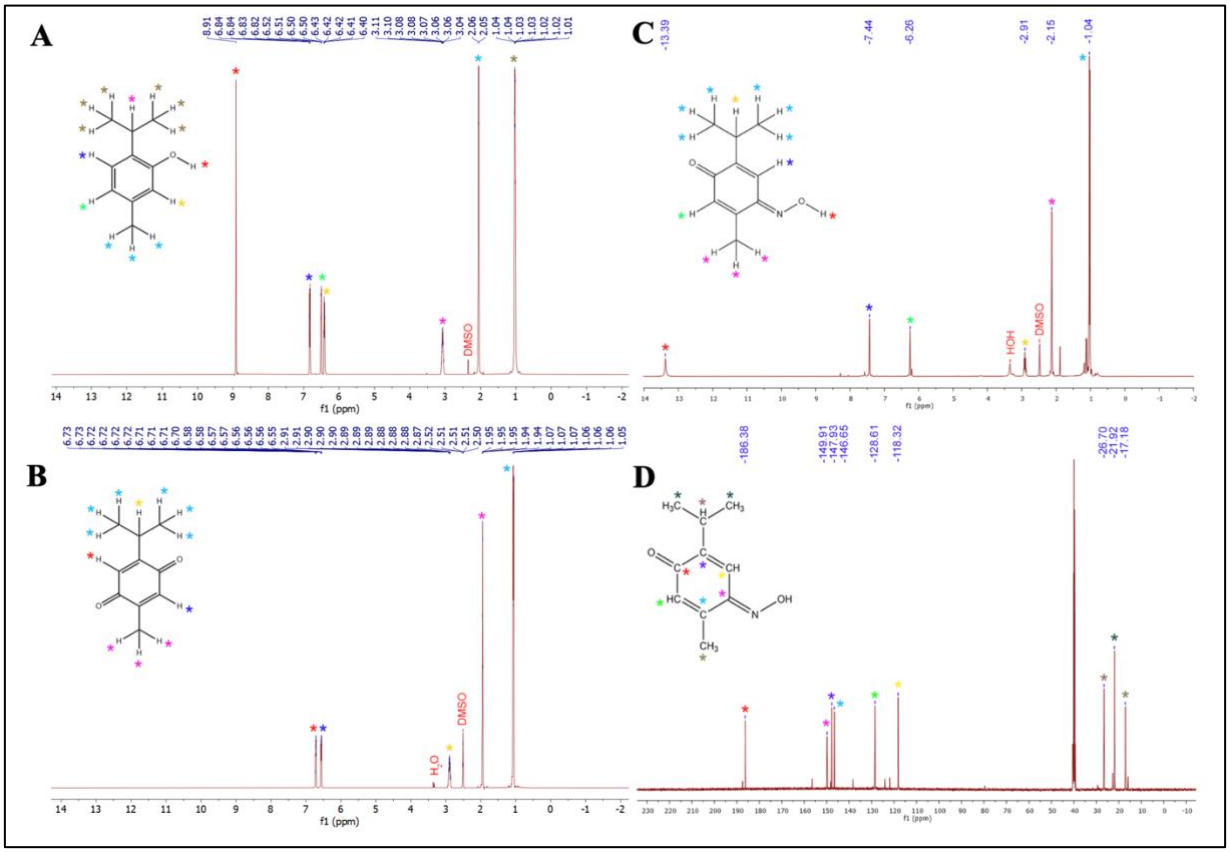


Figure S1. A) The H-NMR spectrum of thymol in DMSO-*d6*. B) The H-NMR spectrum of thymoquinone in DMSO-*d6*. C) The H- and D) C-NMR spectra of thymoquinone-oxime in DMSO-*d6*.

Figure S2

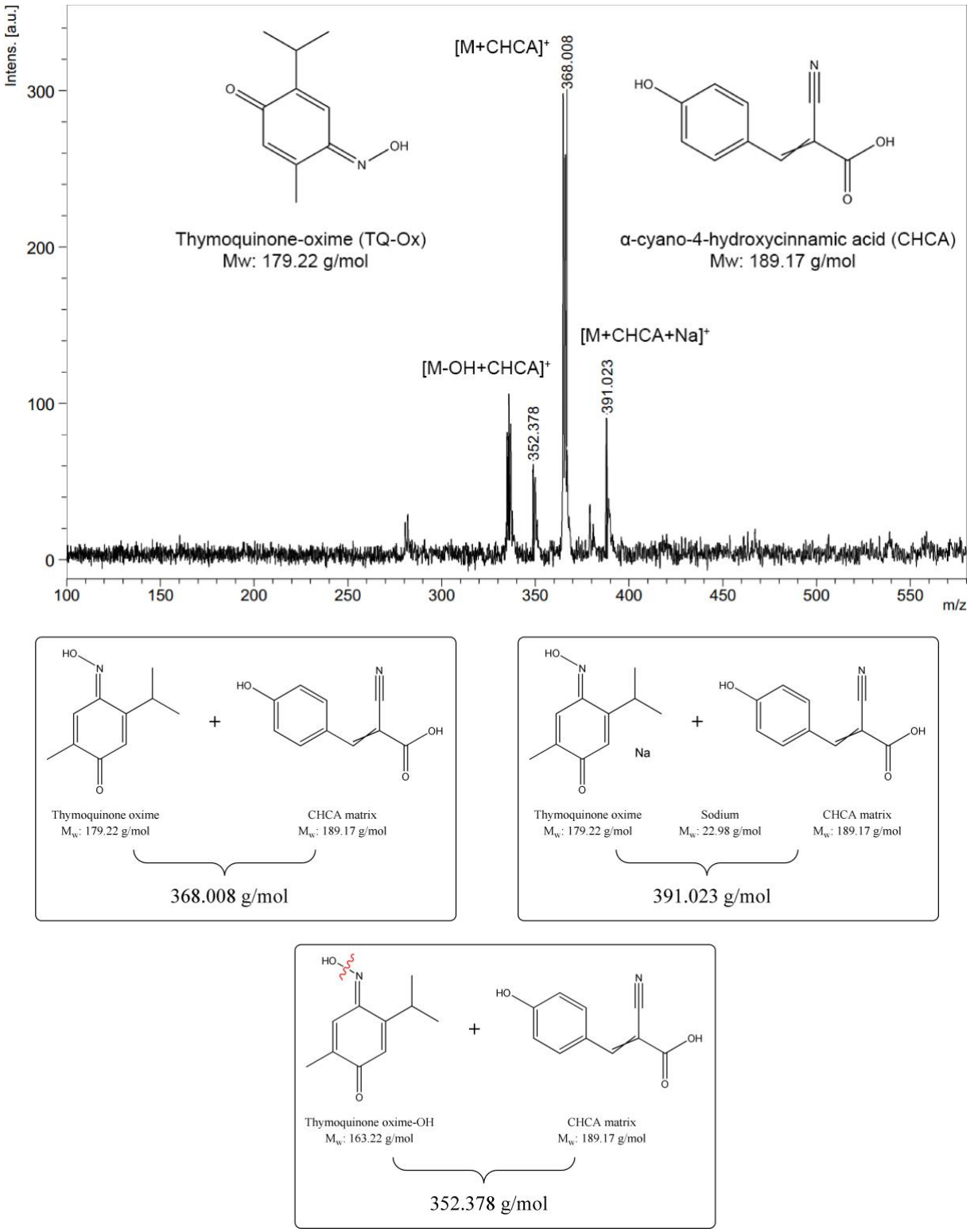


Figure S2 The MALDI-TOF mass spectrum of thymoquinone-oxime using CHCA matrix.

Figure S3

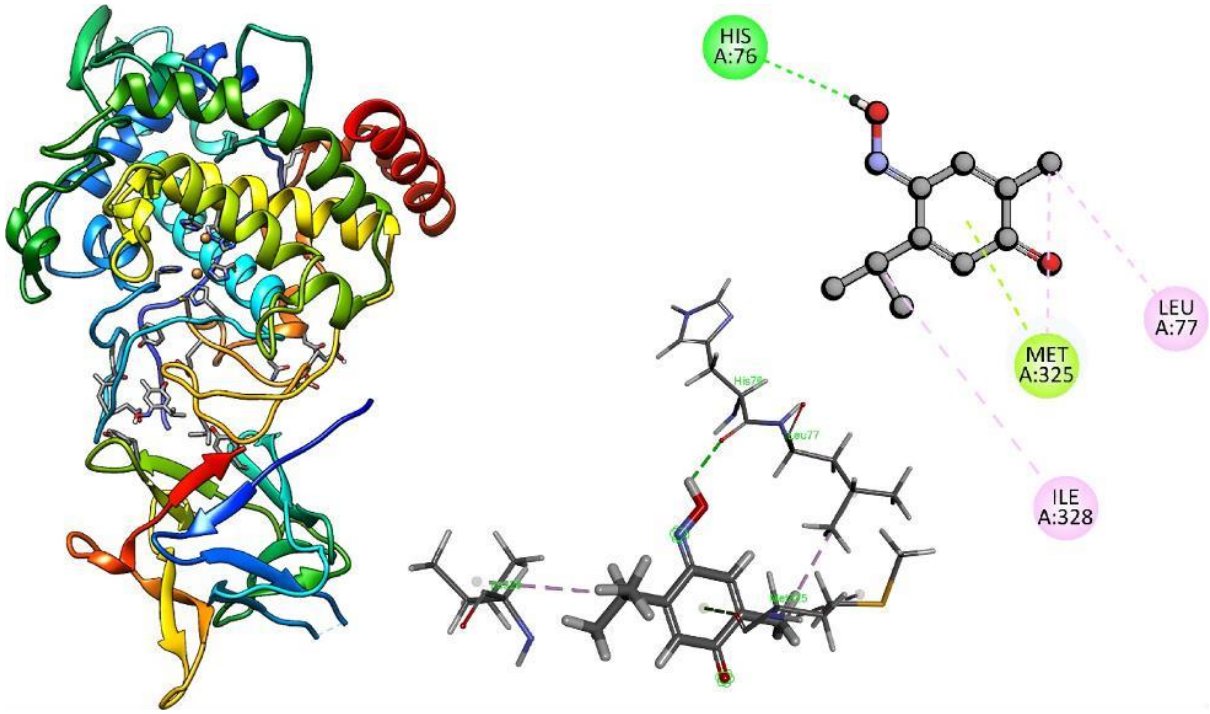


Figure S3 The molecular docking results of thymoquinone-oxime (TQ-Ox) and Tyrosinase enzyme (PDB: 2Y9W).

Figure S4

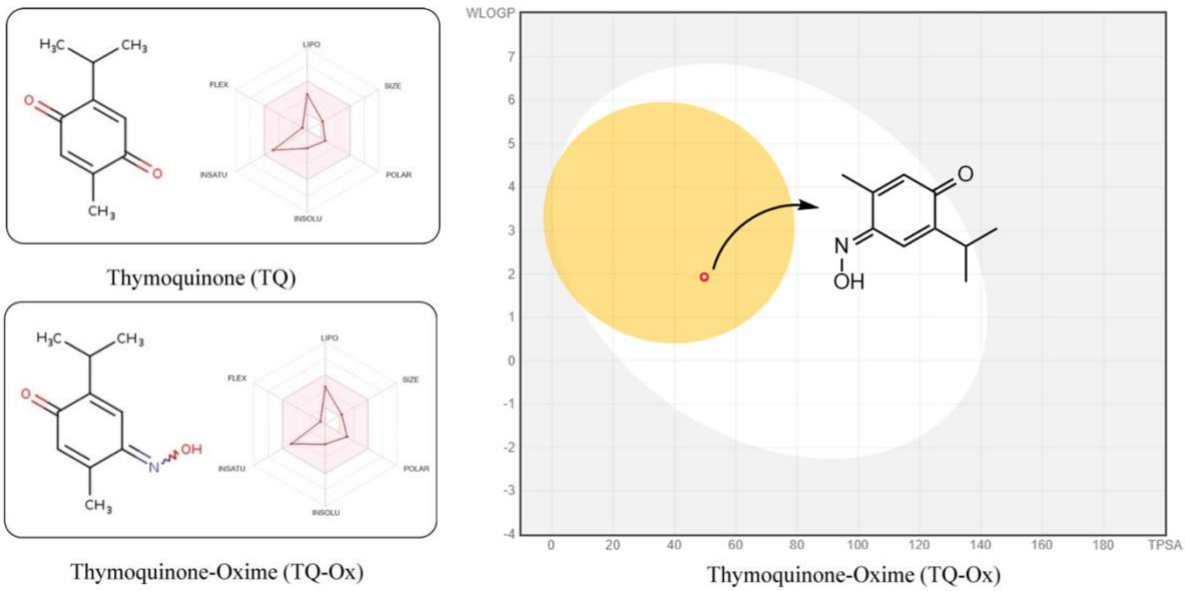


Figure S4 Pharmacokinetic properties of thymoquinone (TQ), thymoquinone-oxime (TQ-Ox), and **b**lood brain barrier permeation of TQ-Ox according to the yolk of the BOILED-Egg.

Figure S5

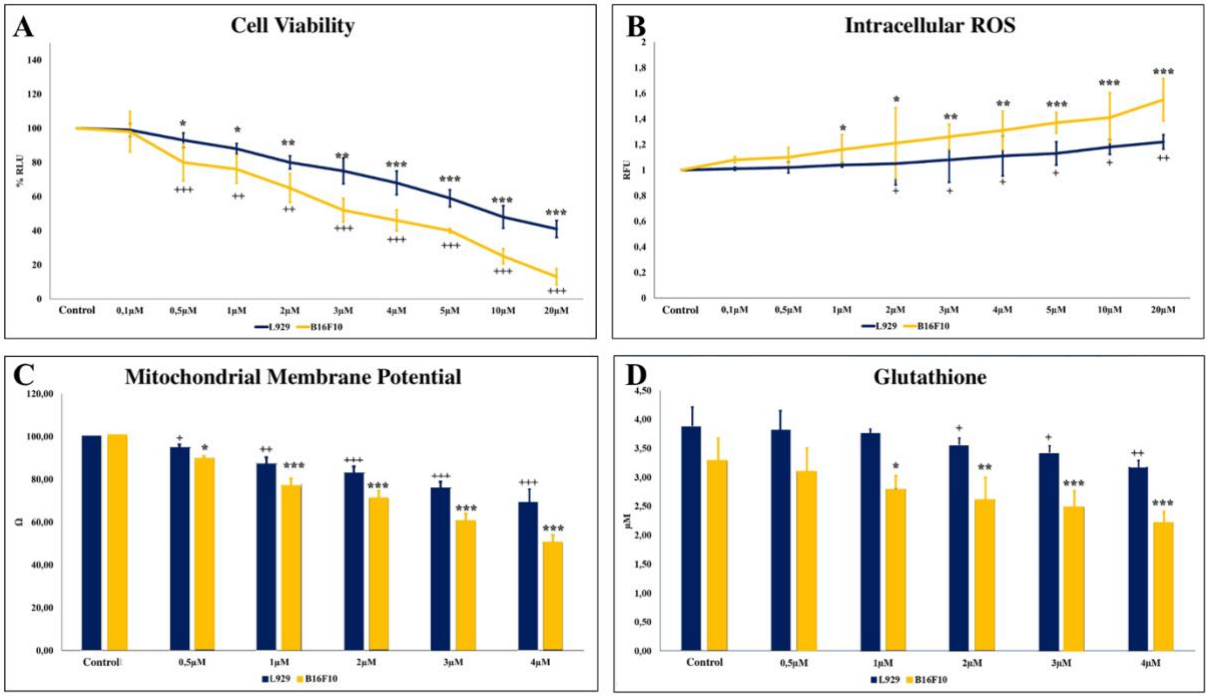


Figure S5 A) The effect of thymoquinone-oxime (TQ-Ox) concentrations (0.5-20 μM) on malignant melanoma (B16F10) and healthy fibroblast (L929) cells viability. The results are expressed as relative luminescence units (RLU). **B**) Intracellular Reactive Oxygen Species (iROS) activity in TQ-Ox concentration 0.5-20 μM. The results are expressed as relative fluorescence units (RFU). **C**) The levels of mitochondrial membrane potential (MMP) of TQOx) concentrations (0.5-4 μM) on cell lines B16F10 and L929. **D**) Intracellular Glutathione (GSH) levels of TQ-Ox concentrations (0.5-4 μM) on cell lines B16F10 and L929. All concentrations are expressed as mean ± SD of four independent replicates., and the statistical differences were expressed according to the control as $^{*}p<0.05$, $^{**}p<0.01$, $^{***}p<0.001$; $^{+}p<0.05$, $^{++}p<0.01$, $^{+++}p<0.001$.

Figure S6

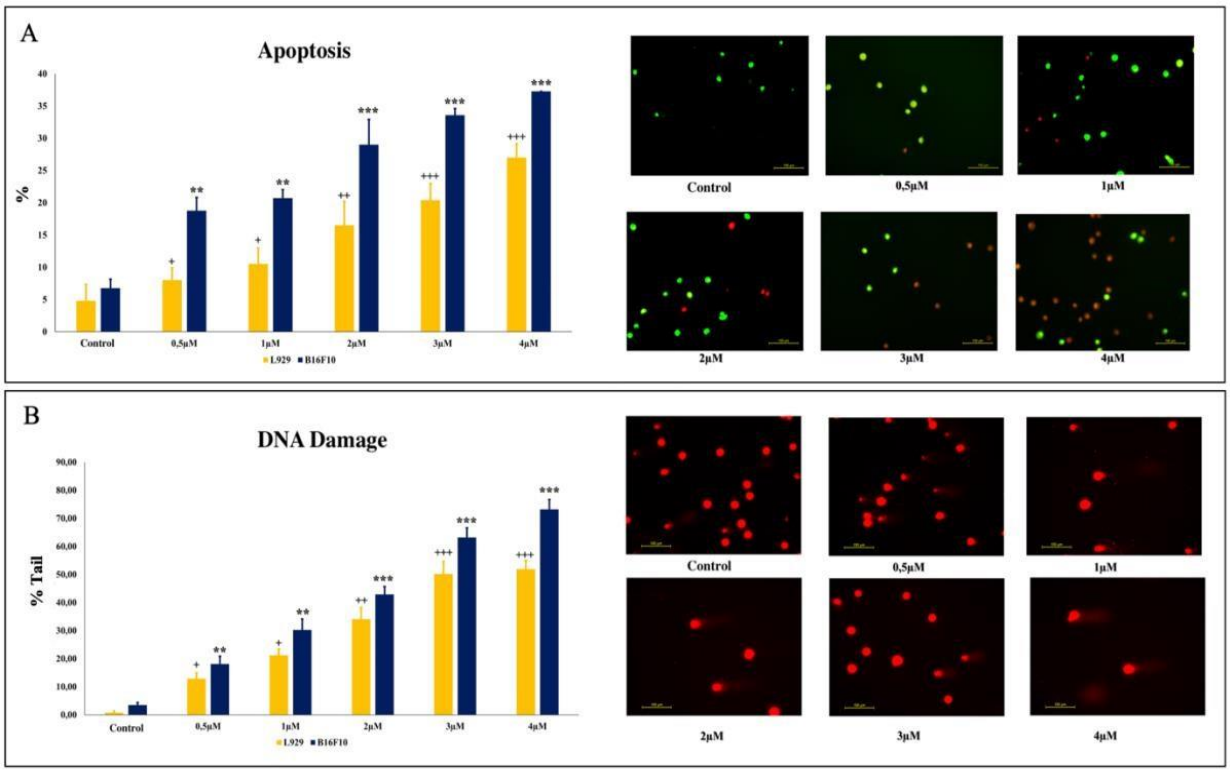


Figure S6 The Thymoquinone-oxime (TQ-Ox) concentrations (0.5-4 µM) on apoptosis and DNA damage in malignant melanoma (B16F10) and healthy fibroblast (L929) cells **A**) Effect TQ-Ox on apoptosis given as % apoptosis and representative immunofluorescence images with AO/EB dual dye. **B**) Effect TQ-Ox on B16F10 and L929 on DNA damage—representative immunofluorescence images of genotoxicity of different concentrations TQ-Ox in B16F10 cell line. Undamaged DNA was rounded, whereas damaged DNA had brilliant nuclei and cometlike nuclei. The comet image in the DNA formed after damage increased as the concentration increased. All results are given the mean ± standard deviation (mean ± SD) of four independent replicates. Differences for the values $^{*}p<0.05$, $^{**}p<0.01$, $^{***}p<0.001$ for B16F10; $^{+}p<0.05$, $^{++}p<0.01$, $^{+++}p<0.001$ for L929 were considered statistically significant.

References

Gour, A., Dogra, A., Verma, M. K., Bhardwaj, M., Kour, D., Jamwal, A., Gorain, B., Kumar, M., Vij, B., & Kumar, A. (2023). Ayurveda-based phytochemical composition attenuates lung inflammation and precipitates pharmacokinetic interaction with favipiravir: an in vivo investigation using disease-state of acute lung injury. *Natural Product Research*, *37*(22), 3758–3765.

McGahon, A. J., Martin, S. J., Bissonnette, R. P., Mahboubi, A., Shi, Y., Mogil, R. J., Nishioka, W. K., & Green, D. R. (1995). The end of the (cell) line: methods for the study of apoptosis in vitro. *Methods in Cell Biology*, *46*, 153–185.

Singh, N. P., Danner, D. B., Tice, R. R., Brant, L., & Schneider, E. L. (1990). DNA damage and rpair with age in individual human lymphocytes. *Mutation Research/DNAging*, *237*(3–4), 123–130.

Tang, X., & Hou, T. (2011). Isolation and identification of 2-isopropyl-5-methylphenol from Stellera chamaejasme and its insecticidal activity against Aphis craccivora and Pieris rapae. *Natural Product Research*, *25*(4), 381–386.